Theoretical Studies of $[Os_3(CO)_{10}(\alpha\text{-Diimine})]$: Structures, Frontier Orbitals and Bonding

Maria José Calhorda,*[a,b] Elke Hunstock,[a] Luís F. Veiros,[c] and František Hartl[d]

Keywords: Osmium / Cluster compounds / DFT calculations / Charge transfer / Molecular orbitals / Diimines

DFT calculations were performed on $Os_3(CO)_{10}$(α-diimine) clusters, for α-diimine = DAB (1,4-diaza-1,3-butadiene), PYCA (σ-*N*,σ-*N*′-pyridine-2-carbaldehyde-imine), and BIPY (2,2′-bipyridine). Geometry optimizations were performed for several models of the possible isomers under different conditions. Axial isomers were always found to be the most stable, in agreement with the available X-ray determined structures. A full optimization of the geometry was required in order to improve the quality of the results, but the distances tended to be longer than the experimental ones. In spite of these shortcomings, the nature of the frontier orbitals, showing the increasing localization of the cluster LUMO in the α-diimine ligand as this is expanded (45, 65, 76% for DAB, PYCA, and BIPY, respectively), was consistent with the increasing MLCT character of the HOMO–LUMO transition along the series. Extended Hückel calculations were able to reproduce these trends qualitatively.

Introduction

There is a significant number of theoretical studies dealing with binary carbonyl transition metal clusters. The $M_3(CO)_{12}$ triad (M = Fe, Ru, Os) has been the object of a very important fraction of such studies, the relevant issue being that the iron derivative exhibits C_{2v} symmetry and has two bridging carbonyls over one edge, while both the ruthenium and the osmium clusters only possess terminal carbonyls. Several levels of theory have been used, starting from semiempirical extended Hückel (EH) and INDO calculations, up to HF and MP2 calculations, and more recently DFT methods.[1] Semiempirical methods can be applied to all clusters, independently of their size and symmetry, and this is their main advantage. On the other hand, more sophisticated methods can give a better answer to specific problems and become more reliable when trying to predict structures of molecules. From our previous experience, it is known that DFT methods are very adequate for dealing with first-row transition-metal clusters, while MP2 becomes the best choice for third-row derivatives. On the other hand, MP2 takes considerable time and requires extensive computer capabilities when studying large systems.[2]

Theoretical studies of mixed clusters containing other ligands besides carbonyls are less common, although they involve much chemistry.[3] The influence of the nature of the ligands on carbonyl bridge formation has been studied and it was found that coordination of π-donors can increase the tendency to form carbonyl bridges in clusters of second-row transition metals, such as ruthenium or rhodium, when they are absent in the binary carbonyl parent cluster.[4] Some publications address the triosmium clusters in detail. Morokuma and co-workers studied the bonding in $Os_3(CO)_9(C_6H_6)$ using single-point MP2 energy calculations on HF-optimized structures, and EH for orbital analysis.[5] Some of us qualitatively analyzed the bonding of *ortho*-metallated α-diimines to $HOs_3(CO)_9$.[6a]

In this work, DFT calculations[7] performed under different conditions and on models of three $Os_3(CO)_{10}$(α-diimine) clusters are described, and the reliability of extended Hückel[8] calculations on these systems is discussed. This study was prompted by the rich photochemistry[9] and intriguing electrochemistry[6] exhibited by these clusters. Di- and trinuclear transition-metal carbonyls with the α-diimine ligand have been found to undergo a photochemical metal−metal bond homolysis from a low-lying σπ* excited state, in which σ represents the metal−metal bonding orbital and π* represents the lowest unoccupied orbital of the α-diimine. This excited state is either directly optically available or can be occupied by surface crossing from the metal-to-α-diimine (MLCT) states.[10] Experimental results indicate that a similar situation also applies to the $Os_3(CO)_{10}$(α-diimine) clusters which produce diradicals in non-coordinating or weakly coordinating solvents upon irradiation with visible light.[9] This knowledge can be used to check the accuracy of our model compounds, as will be discussed later.

[a] ITQB, Quinta do Marquês, EAN, Apart. 127, 2781-901 Oeiras, Portugal
[b] Departamento de Química e Bioquímica, Faculdade de Ciências, Universidade de Lisboa, 1749−016 Lisboa, Portugal
[c] Centro de Química Estrutural, IST, Av. Rovisco Pais, 1049-001 Lisboa, Portugal
[d] Universiteit van Amsterdam, Institute of Molecular Chemistry, Nieuwe Achtergracht 166, 1018 WV Amsterdam, The Netherlands

  1434−1948/01/0101−0223 $ 17.50+.50/0

Results and Discussion

Molecular Structures

Three model α-diimine ligands were considered in this work, namely DAB (1,4-diaza-1,3-butadiene), PYCA (σ-*N*,σ-*N*′-pyridine-2-carbaldehyde-imine), and BIPY (2,2′-bipyridine), as depicted in Scheme 1. They differ by the progressive replacement of the imine C=N bonds by pyridine rings.

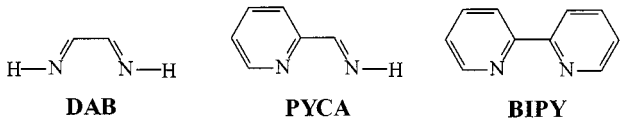

Scheme 1

The $Os_3(CO)_{10}$(DAB) cluster (**1**) was the first to be studied (see Experimental Section for details) and the availability of the X-ray structure of the related $Os_3(CO)_{10}$(*i*Pr-DAB)[11] provided a good starting point for the calculations. In principle, two alternative structures are possible for this cluster with the α-diimine σ-*N*,σ-*N*′-chelated to a single osmium atom, namely the axial and the equatorial one, as depicted in Scheme 2, left and right.

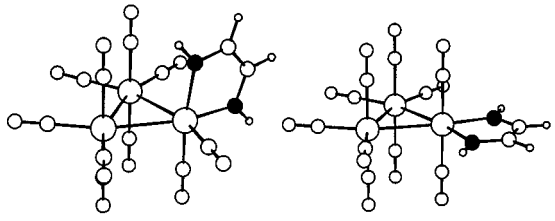

Scheme 2

The axial isomer (left) has no symmetry (C_1), while the equatorial isomer has two mirror planes and a twofold rotation axis. The first model was very similar to what can be seen in Scheme 2, since the terminal carbonyl groups were forced to lie on the Os3 plane or to be perpendicular to it. The other variables were optimized. The axial isomer (**1aL**) was found by DFT calculations to be more stable by 0.83 eV. A relatively large basis set (see basis set L in Experimental Section) was used for these two initial calculations. A reduced basis set (see Experimental Section) was used afterwards (**1a**) because the size of the other ligands (PYCA and BIPY) prevented the use of the larger one. Obviously, the same conditions must be used in order to compare results for the three α-diimine ligands. Extended Hückel calculations[8] led to a similar result, namely that the axial isomer was more stable by 0.75 eV.

The features of the rigid models **1aL** and **1a** significantly deviated from those of the available crystal structure of $Os_3(CO)_{10}$(*i*Pr-DAB). Besides the distances, to which we shall come back, the angles were totally different. Therefore, the model for the more stable axial isomer was improved, making it more flexible by allowing all the torsion angles to vary (**1b**). The calculated DFT energy dropped by 0.71 eV. A single-point calculation was also performed using the coordinates of the experimental structure (**1c**). The energies cannot be compared, as there are two isopropyl substituents on the DAB nitrogen atoms. However the nature of the frontier orbitals should be similar if the model is reliable, and calculated and experimental bond lengths can therefore be compared. The geometry of the axial isomer, with C_1 symmetry, was also optimized using *Gaussian 94*[12] (**1d**; HF; see Experimental for details). A general idea of the structural differences between the five calculations of the axial isomer can be inferred from the drawings in Scheme 3, showing the rigid model (**1a**), the more flexible model (**1b**), the experimental structure on the top right (**1c**), the rigid model (basis set L; **1aL**), and the flexible model (Gaussian; **1d**).

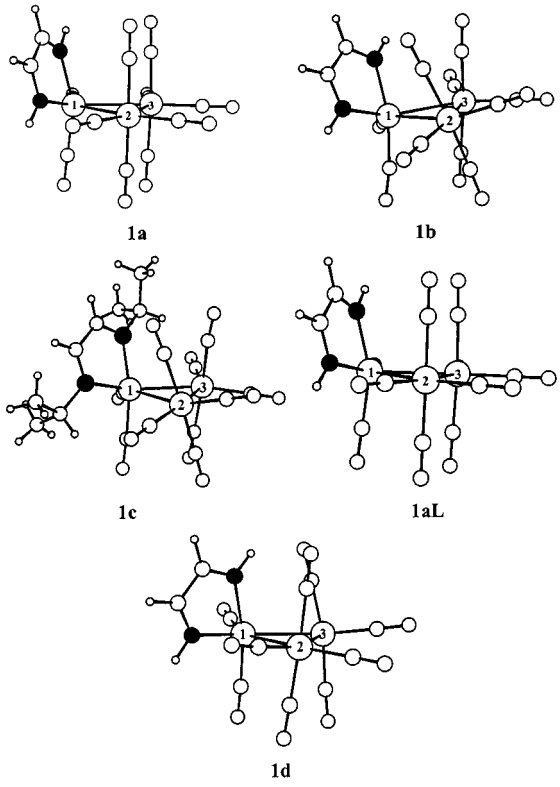

Scheme 3

The most relevant distances (Os−Os and Os−N) are listed in Table 1, and while the main features of the observed structure are reproduced in the calculations, the distances tend to be too long when DFT methods are used (**1a, 1b**). Although only the HF approach could be used owing to the size of the cluster, the distances (**1d**) are in

Table 1. Selected distances (pm) in several models and calculation levels of $Os_3(CO)_{10}$(DAB) (**1a, 1aL, 1b, 1d**) and in $Os_3(CO)_{10}$(*i*Pr-DAB) (**1c**)

Bond/Model	**1a**	**1aL**	**1b**	**1c** (exp.)	**1d**[a]
Os1−Os2	305.0	303.2	297.9	287.7	292.3
Os1−Os3	301.6	301.3	300.6	288.0	292.5
Os2−Os3	303.7	304.6	299.9	286.7	296.9
Os1−N1	212.0	210.9	213.7	211.4	215.5
Os1−N2	212.0	210.9	209.3	206.6	207.3

[a] HF calculations.

better agreement with the experimental ones (**1c**), especially with respect to the Os−Os bonds.

The first two columns in Table 1 demonstrate the effect of the basis set. The larger one (**1aL**) leads to shorter distances, but exceeded our computing capabilities when we moved to the larger α-diimine ligands. A comparison of the values in columns **1a** and **1b** shows, however, that the effect of using a better model is more important. Indeed, the full geometry optimization is more effective in reducing bond lengths than increasing the basis set. For instance, Os1−Os2 drops from 305.0 pm in **1a** to 303.2 in **1aL** with the better basis set, but to 297.9 pm in **1b**, with a better model and a small basis set, getting closer to the experimental value of 287.7 pm (**1c**).When the same model is used and one compares DFT and HF, it can be seen that this last method leads to shorter Os−Os bond lengths. The computation time is increased, though, and one of the Os−N bonds is even longer. The size and lack of symmetry of compound **1** precluded an MP2 calculation, although recent calculations on the more symmetric $Os_3(CO)_{12}$ showed MP2 to reproduce distances better.[2]

Another interesting aspect of the experimental structure, also reproduced by the full optimization procedure, concerns the torsion angles around the carbonyl groups. Although a list of their values is of limited value, it can be noted that some of them move away from the perpendicular to the Os3 plane by up to 25°, as clearly seen in Scheme 3. The HF structure (**1d**) has bond lengths in good agreement with the experimental structure (**1c**), but the torsion angles are very different, and the carbonyls bend in the wrong direction, revealing the limitations of this approach. The overall picture provided by the DFT-optimized structure is more realistic, despite the long bond lengths.

The introduction of the first pyridine ring changes DAB into PYCA (Scheme 1). As the ligand is asymmetric, there are more possible isomers for the model compound $Os_3(CO)_{10}$(PYCA) (**2**), as the two axial isomers (**2a1, 2a2**) shown in Scheme 4 (top and center) are not equivalent. The equatorial isomer (**2a3**) is the more symmetric one, with a mirror plane (C_s).

There is no X-ray structure available for compound **2** or a related one. DFT calculations with the standard basis set, keeping the carbonyls perpendicular to or on the Os_3 plane, were performed for the three isomers. The most stable is the axial isomer **2a1**. The other axial isomer **2a2** has a higher energy (0.18 eV), while the equatorial **2a3**, with an energy 0.31 eV higher than **2a1**, is the least stable. For this $Os_3(CO)_{10}$(PYCA) cluster, EH calculations showed the axial species **2a2** to be the most stable, followed by **2a3** (0.28 eV) and **2a1** (2.23 eV). This result can be traced to steric repulsion between the pyridine ring of the ligand and the carbonyls perpendicular to the Os_3 plane, as no geometry optimization was made. The DFT calculations, allowing for these repulsions to be relieved during the geometry-optimization process, led to a more likely order of stability, with **2a1** being the most stable isomer.[13] Also, since the carbonyl groups are much stronger π-acceptors than the α-diimines, *cis*-$Os_3(CO)_2$ geometries (as in the axial isomers) are more stable than structures with carbonyls in *trans* positions (the equatorial isomer) competing for π back donation from the same metal orbitals.

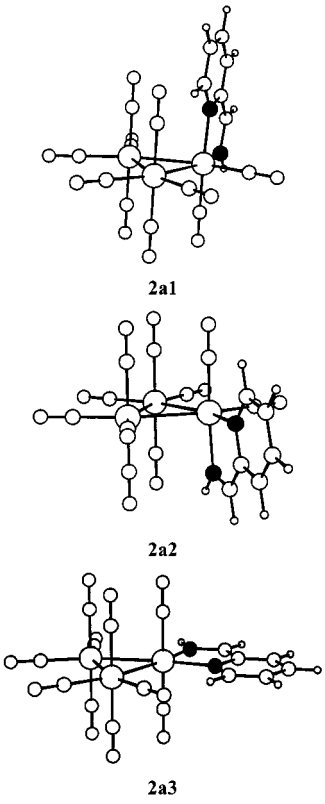

Scheme 4

A full optimization of the axial isomer (**2b**), taking all the degrees of freedom into account, resulted in a more stable cluster (0.94 eV), as expected from the study of the DAB derivatives. A complete geometry optimization using Gaussian94 HF, was also performed (**2d**). The representation of the geometries clarify the changes in the carbonyl positions which take place as the model improves (Scheme 5). The relevant distances are given in Table 2.

These distances can be compared with those of $Os_3(CO)_{10}$(*i*Pr-DAB) given in Table 1. The conclusions are similar to those drawn above, namely that DFT methods give too long distances. The HF calculation leads to shorter Os−Os bonds, but on the other hand one of the Os−N bonds is the largest. Interestingly, for this system, the carbonyls occupy the same positions as in the DFT-optimized structures and in $Os_3(CO)_{10}$(*i*Pr-DAB), in opposition to what was found for the model DAB cluster.

The third cluster studied was $Os_3(CO)_{10}$(BIPY) (**3**). There are two isomers, an axial and an equatorial one, similar to those in Scheme 2. A complete optimization of both isomers was performed using DFT calculations, and the axial isomer was found to be more stable by 0.52 eV. The drawings of the optimized structures of the (**3b1**) axial and equatorial (**3b2**) isomers and the X-ray structure of $Os_3(CO)_{10}$(BIPY) (**3c**)[14] are represented in Scheme 6. Both the calculated Os−Os and Os−N distances are too long compared with the observed ones (Table 3).

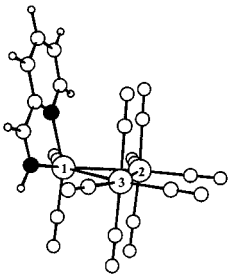

2a1

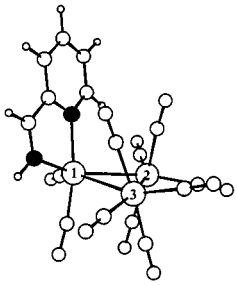

2b

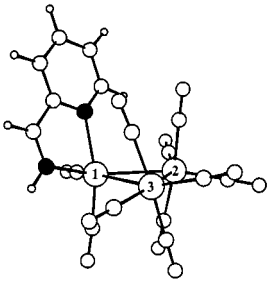

2d

Scheme 5

Table 2. Selected distances (pm) in several models and calculation levels of $Os_3(CO)_{10}$(PYCA) (**2a1, 2b, 2d**)

Bond/Model	**2a1**	**2b**	**2d**[a]
Os1−Os2	308.6	293.7	289.6
Os1−Os3	300.6	304.1	296.6
Os2−Os3	300.2	297.2	297.1
Os1−N1	217.3	222.5	226.3
Os1−N2	217.3	211.9	211.7

[a] HF calculations.

Since the geometry of the two isomers of $Os_3(CO)_{10}$(BIPY) was fully optimized, they can be compared more reliably. From the two drawings in Scheme 6, it can be seen that the carbonyls do not need to distort so much away from directions perpendicular to the Os3 plane in the case of the equatorial isomer. This reflects a smaller number of steric repulsive interactions in the axial isomer of the cluster. This steric constraints are reflected in the EH relative energies of the two isomers (idealized geometries with carbonyls perpendicular or in the plane of Os_3): the axial isomer is less stable by 2.07 eV. If the carbonyls are allowed to bend back, away from the α-diimine ligand, the energy immediately starts to drop. It is worth noting that in the DAB cluster, where steric repulsions are negligible, the axial

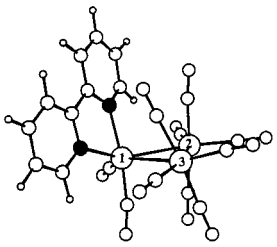

3b1

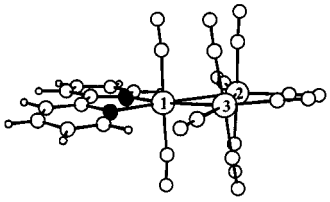

3b2

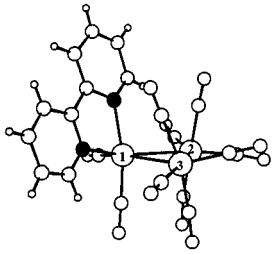

3c

Scheme 6

Table 3. Selected distances (pm) in the axial (**3b1**) and equatorial (**3b2**) isomers of $Os_3(CO)_{10}$(BIPY) and in the experimental structure (**3c**).

Bond/Model	**3b1**	**3b2**	**3c**
Os1−Os2	292.2	301.9	284.1
Os1−Os3	309.5	301.1	290.1
Os2−Os3	297.7	303.8	288.4
Os1−N1	219.8	219.4	217.9
Os1−N2	220.3	220.3	209.0

isomer was found to be the most stable by EH calculations. The introduction of the pyridine rings reverses this pattern and demands further optimization of the geometry (as done in the DFT calculations).

The Os−Os distances are the same in $Os_3(CO)_{10}$(BIPY) and in $Os_3(CO)_{10}$(*i*Pr-DAB) within experimental error, so that any of them can be used to check the calculations on $Os_3(CO)_{10}$(PYCA).

A Qualitative View of the Bonding

The three α-diimine ligands DAB, PYCA, and BIPY have an increasingly large π-system. The bonding of DAB to the cluster is achieved by σ-donation from the two equivalent nitrogen lone-pair orbitals, as the symmetric and antisymmetric combinations, to empty cluster orbitals localized in Os1. There is also a back-donation component from the cluster to the second π* (DAB), LUMO. The set of π orbitals of DAB is very similar to that of 1,3-butadiene, taking into account the different electronegativities of carbon

and nitrogen. The interaction between DAB and $Os_3(CO)_{10}$ is depicted on the right hand side of Figure 1 (EH calculations). The corresponding interaction with PYCA is shown on the left hand side.

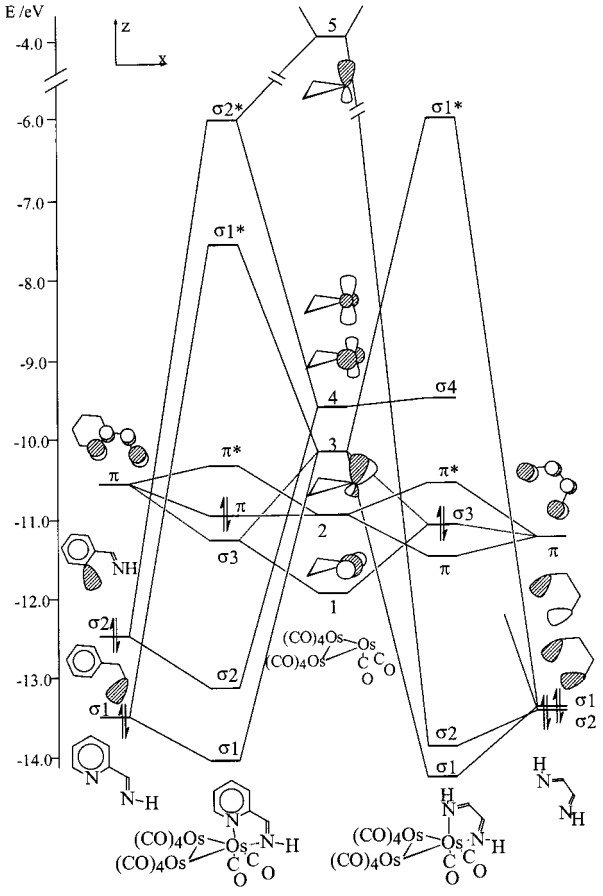

Figure 1. Molecular orbital diagram between the cluster fragment $Os_3(CO)_{10}$ (center) and DAB (right) or PYCA (left), showing the most relevant interactions

The presence of the pyridine ring lifts the degeneracy between the two nitrogen lone pairs. The π* (PYCA) LUMO, the acceptor orbital, is largely localized on the same atoms as in DAB, but lies at higher energy owing to the larger number of nodes (not shown). As a consequence, the LUMO of the triosmium clusters, which is the antibonding combination arising from this back-donation component involving π* (PYCA), is expected to possess different a character in the two clusters. In $Os_3(CO)_{10}$DAB, the energy match is better, the interaction stronger, the covalent character more pronounced, and the levels are delocalized between the carbonyl−osmium fragment and the DAB ligand. For $Os_3(CO)_{10}$PYCA, the energy match is not as good, and the cluster LUMO is much more located on the π* (PYCA) orbital (closer in energy) than on the cluster core. The trend is qualitatively the same as one moves to BIPY. The corresponding π* (BIPY) LUMO lies at a higher energy than that of PYCA, and the cluster LUMO becomes even more localized on the BIPY ligand. We come back to these features in the next section.

The Frontier Orbitals (DFT) and the MLCT Transition

As was discussed above, the agreement between experimental and calculated structures using DFT methods improves when the model is improved and a full optimization is performed. The other feature associated with the different models which changes significantly is the composition of the frontier orbitals. This is of great importance because one of the aims of the present study is to understand and compare the character of the lowest-energy electronic transition in the three investigated clusters, and a reliable way of determining that orbital composition is essential.

The results for the $Os_3(CO)_{10}$(DAB) models compared with those of the experimental structure are given in Table 4.

Table 4. Composition of the frontier orbitals (%) of two models of $Os_3(CO)_{10}$(DAB) (**1a, b**) and of $Os_3(CO)_{10}$(*i*Pr-DAB) (**1c**)

	1a			**1b**				**1c**		
m.o.	Os1	Os2,3	DAB	Os1	Os2,3	DAB	m.o.	Os1	Os2,3	DAB
75a	23	10	26	20	15	16	93a	18	12	13
74a[a]	11	24	21	11	17	45	92a[a]	8	12	53
73a[b]	20	12	39	15	17	39	91a[b]	15	19	33
72a	57	7	16	14	44	3	90a	21	26	14
71a	20	41	5	32	21	9	89a	12	41	2
70a	40	21	12	48	19	9	88a	57	10	13

[a] LUMO. − [b]HOMO.

There is a striking difference in the composition of the LUMO, as one moves from the more primitive (**1a**), to the better model (**1b**), and to the real structure (**1c**). The LUMO becomes much more localized on the DAB ligand, going from only 21%, to 45%, and 53%, the last two numbers being comparable. The HOMO is not as sensitive to the type of model.

Table 5. Composition of the frontier orbitals (%) of two models of $Os_3(CO)_{10}$(PYCA) (**2a1, 2b**)

	2a1			**2b**		
m.o.	Os1	Os2,3	PYCA	Os1	Os2,3	PYCA
84a	22	12	24	23	18	11
83a[a]	8	19	40	7	11	65
82a[b]	22	15	34	18	21	28
81a	10	59	10	21	34	4
80a	27	33	6	23	33	7
79a	33	30	8	49	21	7

[a] LUMO. − [b] HOMO.

Table 6. Composition of the frontier orbitals (%) of the model and the observed structure of $Os_3(CO)_{10}$(BIPY) (**3b1, c**)

	3b1			**3c**		
m.o.	Os1	Os2,3	BIPY	Os1	Os2,3	BIPY
93a	18	17	30	1	1	96
92a[a]	5	7	76	3	3	87
91a[b]	20	24	19	21	23	13
90a	25	29	5	19	29	9
89a	23	34	7	11	40	7
88a	51	20	4	56	15	6

[a] LUMO. − [b] HOMO.

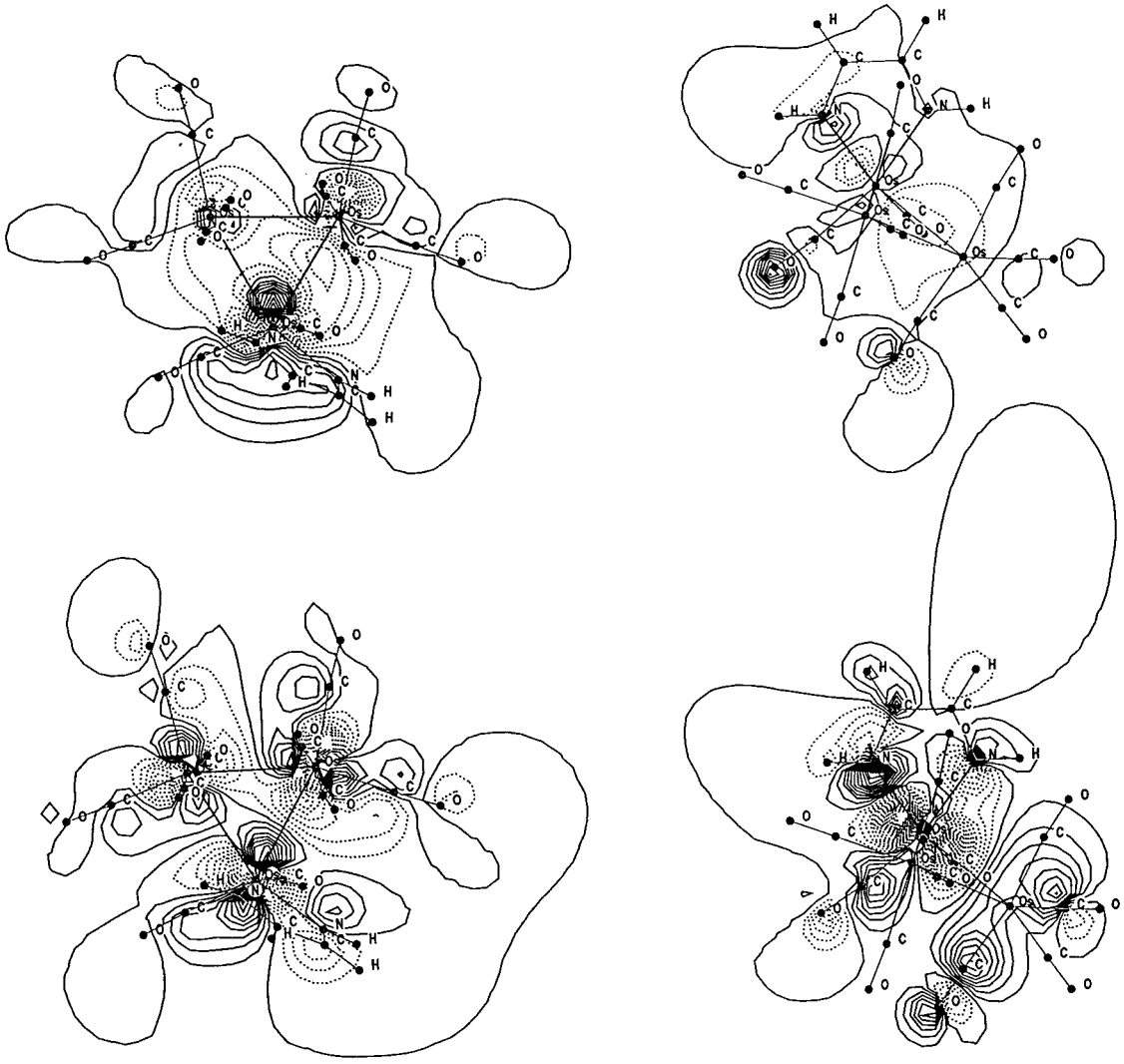

Figure 2. Wavefunction contour plots of the HOMO (top) and LUMO (bottom) of $Os_3(CO)_{10}$(DAB) (**1b**), in the Os_3 plane (left) and in the N−Os−N plane (right)

The same behavior has been found for the $Os_3(CO)_{10}$-(PYCA) cluster (Table 5).

It can be seen that the LUMO has only a contribution of 40% of the ligand in the primitive model, which increases to 65% in **2b**. Conversely, the ligand contribution to the HOMO drops. There is no structure of the cluster, so these values cannot be checked. For $Os_3(CO)_{10}$(BIPY) (Table 6) only the best model (**3b1**) was calculated (full optimization) and there is an experimental structure (**3c**).

There is a good agreement between the composition of the orbitals of the model and of the observed structure, suggesting that our model, in spite of its limitations with regard to the reproduction of bond lengths, describes accurately the nature of the frontier orbitals.

The character of the frontier orbitals can be seen in a better way in the two-dimensional wavefunction plots of Figure 2. In two-dimensional plots, a convenient plane to plot the wavefunction contours must be chosen. In the $Os_3(CO)_{10}$(α-diimine) clusters, the relevant planes are those defined by N−Os−N and by Os_3. We show in Figure 2 both the HOMO and the LUMO for $Os_3(CO)_{10}$(DAB) (**1b**), as two-dimensional plots in the Os_3 plane (left) and in the N−Os−N plane (right).

The same representation is given for $Os_3(CO)_{10}$(BIPY) (**3b1**), in order to compare the character of the orbitals (Figure 3).

The relative energies of the molecular orbitals are also important for the analysis of the electronic transitions. They also depend on the model used to describe the cluster, as can be seen from the selection given in Table 7, for models of $Os_3(CO)_{10}$(DAB) (**1a, 1b**) and $Os_3(CO)_{10}$(*i*Pr-DAB) (**1c**). The HOMO−LUMO gap is 1.76 eV for $Os_3(CO)_{10}$(*i*Pr-DAB) (**1a**), close to the value obtained for the flexible model **1b** (1.66 eV), but much larger than the result obtained with the rigid model **1a** (1.46 eV).

Finally, in Table 8 we give the relative energies of the frontier orbitals for the flexible models of the axial isomers of the three clusters (**1b, 2b, 3b1**) and $Os_3(CO)_{10}$(BIPY). The HOMO−LUMO gap varies with the α-diimine ligand, going from 1.66 eV for the DAB cluster, to 1.50 eV for the

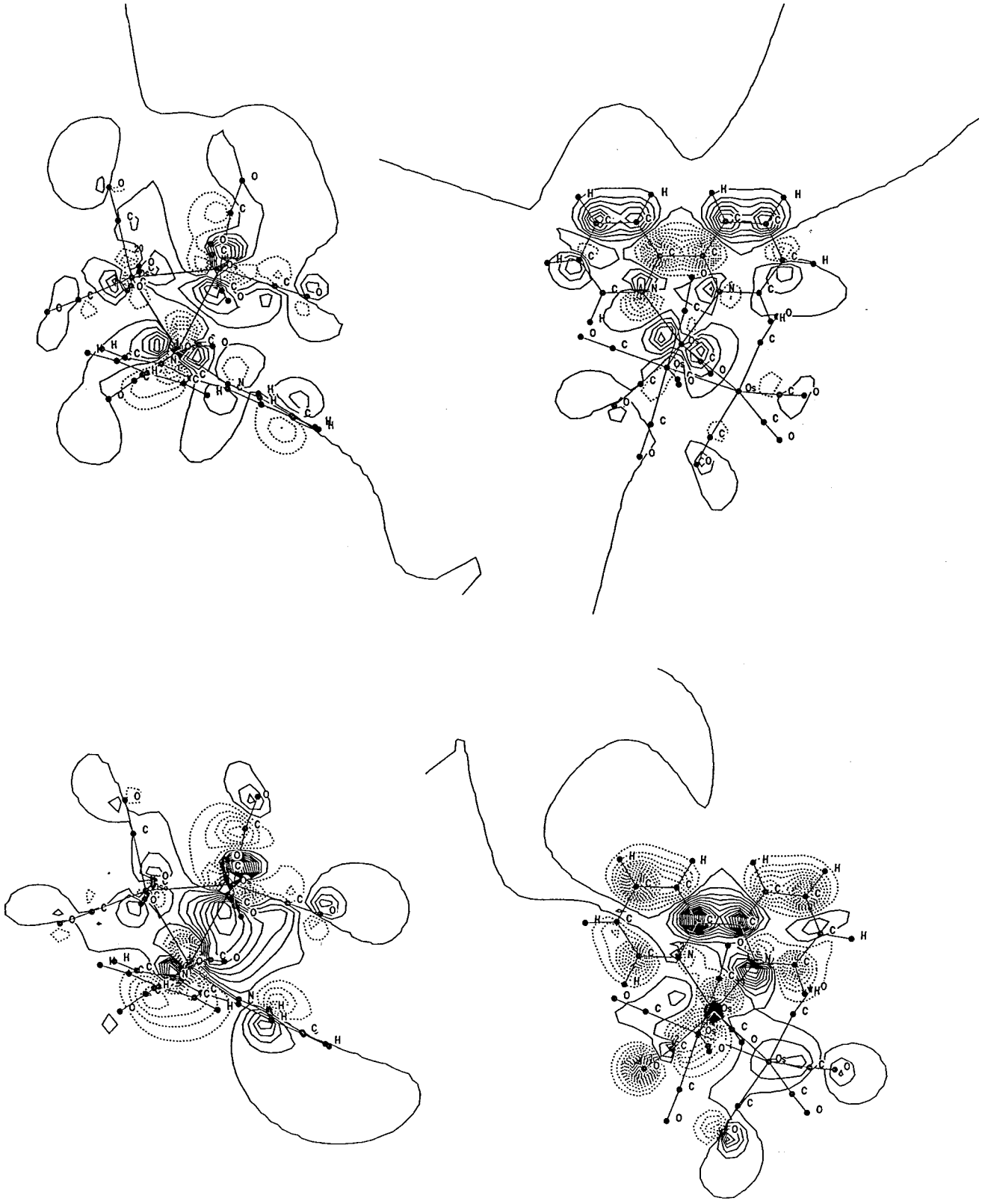

Figure 3. Wavefunction contour plots of the HOMO (top) and LUMO (bottom) of $Os_3(CO)_{10}$(BIPY) (**3b1**), in the Os_3 plane (left) and in the N−Os−N plane (right)

PYCA cluster, and 1.41 eV for the BIPY cluster. It becomes smaller as the HOMO becomes more localized in the metals and the LUMO in the diimine.

Final Remarks

As discussed above, the LUMO becomes progressively more localized on the α-diimine ligand as one moves from

Table 7. Energies of the frontier orbitals (eV) of models of $Os_3(CO)_{10}$(DAB) (**1a, 1b**) and $Os_3(CO)_{10}$(*i*Pr-DAB) (**1c**)

	1a	**1b**		**1c**
m.o.			m.o.	
75a	−3.28	−3.24	93a	−2.72
74a[a]	−3.76	−3.99	92a[a]	−3.51
73a[b]	−5.22	−5.65	91a[b]	−5.27
72a	−5.70	−6.01	90a	−5.65
71a	−6.03	−6.07	89a	−5.70
70a	−6.33	−6.43	88a	−6.12

[a] LUMO. – [b] HOMO.

Table 8. Energies of the frontier orbitals (eV) of models of $Os_3(CO)_{10}$(α-diimine) (**1b, 2b, 3b1**) and $Os_3(CO)_{10}$(BIPY) (3**c**)

	1b	**2b**		**3b1**	**3c**
m.o.		m.o.		m.o.	
75a	−3.24	84a	−3.17	93a	−3.15	−3.06
74a[a]	−3.99	83a[a]	−3.89	92a[a]	−3.72	−3.74
73a[b]	−5.65	82a[b]	−5.39	91a[b]	−5.13	−5.16
72a	−6.01	81a	−5.83	90a	−5.66	−5.51
71a	−6.07	80a	−5.89	89a	−5.80	−5.55
70a	−6.43	79a	−6.39	88a	−6.26	−6.23

[a] LUMO. – [b] HOMO.

DAB, to PYCA, to BIPY in $Os_3(CO)_{10}$(α-diimine) (45, 65, 76% from **1b, 2b, 3b1**, respectively) and the HOMO on the metal-carbonyl core (32, 39, 44%), indicating that the cluster core-to-ligand charge-transfer character of the HOMO−LUMO transition increases along the series. This trend agrees well with the previously published resonance Raman spectra of the clusters $Os_3(CO)_{10}$(α-diimine) (α-diimine = *i*Pr-DAB, *i*Pr-PYCA, BIPY).[9a][9b] The spectra document that in the case of the *i*Pr-DAB-derivative, the HOMO−LUMO transition possesses a pronounced metal−ligand bonding-to-antibonding rather than charge-transfer character, in agreement with its negligible solvatochromism.[15] For the *i*Pr-PYCA and BIPY-derivatives, the resonance Raman spectra and negative solvatochromism[9b] manifest a significant charge transfer character of this first electronic transition. This difference is also reflected in the limited tendency of the clusters $Os_3(CO)_{10}$(R-DAB) (R = alkyl) to produce charge-separated zwitterions from the diradical intermediates photogenerated upon the HOMO−LUMO excitation, in sharp contrast to the photochemistry of the R-PYCA and, in particular, BIPY-derivatives.[9a] Such conversion demands localization of the excited electron mainly in the π* orbital of the α-diimine ligand, which is not the case in the strongly π-delocalized Os−DAB metallacycle (see Table 4, model **1b**).

The extended Hückel method does not give a good result for predicting relative energies of isomers, in the absence of a geometry optimization, but leads to a good description of the nature of the frontier orbitals, reflecting the progressive contribution of the α-diimine ligand to the LUMO and of the three osmium atoms to the HOMO in the $Os_3(CO)_{10}$(α-diimine) clusters.

Experimental Section

All Density Functional Theory calculations were performed using the Amsterdam Density Functional program package (ADF).[17,18] The Local Spin Density (LSD) exchange correlation potential was used with the Local Density Approximation of the correlation energy (Vosko−Wilk-Nusair).[19] Gradient-corrected geometry optimizations were performed using Becke's[20] exchange and Perdew's[21] correlation functionals, and included relativistic effects, treated by a quasi-relativistic method where Darwin and mass-velocity terms are incorporated.[23]

The inner shells of Os (1s−5p) were frozen, for both the large (L) and reduced basis sets. A triple-ζ STO basis set was used for the valence part of Os (5d−6s), additionally augmented by one diffuse 6p function. For C and N, the 2s and 2p valence shells were described by a triple-ζ STO basis, augmented by one 3d polarization function. For O and H a double-ζ STO basis was used. In the large (L) case, the 2s and 2p shells of C, O and N and the 1s shell of H are triply split and augmented by two polarization functions (3d+4f for C, O, N; 2p+3d for H).

The Hartree−Fock (HF) geometry optimizations were performed using Gaussian94.[12] For Os, the inner shells (1s−4f) were replaced by relativistic effective core potentials of Hay and Wadt,[24] thus including the outermost core orbitals into the SCF procedure. These orbitals were fully contracted while the valence shells were described by a double-ζ STO basis completed by two additional diffuse 6p functions.[25] For the ligand atoms C, O, N and H, standard basis sets (6−31G) were used. The geometry optimizations were performed without any symmetry constraints, except for the equatorial isomers (C_s symmetry).

The extended Hückel method with modified H_{ij} values was used.[26] The basis set for the metal atoms consisted of *n*s, *n*p and (*n-1*)d orbitals. The s and p orbitals were described by single Slater-type wavefunctions, and the d orbitals were taken as contracted linear combinations of two Slater-type wavefunctions. The parameters used for Os were (H_{ii}/eV, ζ): 6s −8.17, 2.452; 6p −4.81, 2.429; 5d −11.84, 5.571, 2.416 (ζ_2), 0.6372 (C_1), 0.5598 (C_2). Standard parameters were used for other atoms. The calculations were performed on model clusters with idealized structures based on the real structures quoted throughout the text. The results were compared with the real structures, when available, producing qualitatively similar results. The bond lengths (Å) were as follows: Os−Os 2.90, Os−C(CO) 1.95, Os−N 2.15, Os−C 2.15, C−O 1.15, C−N 1.40, C−C 1.40, C−H 1.08, N−H 1.08.

Acknowledgments

M. J. C. and E. H. gratefully acknowledge funding from the TMR Network "Metal Clusters in Catalysis and Organic Synthesis". This work is also part of a European collaboration COST Action D14, project D14/0001/99.

[1] [1a] B. E. R. Schilling, R. Hoffmann, *J. Am. Chem. Soc.* **1979**, *101*, 3456. – [1b] J. Li, K. Jug, *Inorg. Chim. Acta.* **1992**, *196*, 89. – [1c] E. J. Baerends, A. Rosa, *New J. Chem.* **1991**, *15*, 815. – [1d] D. G. J. Evans, *J. Chem. Soc., Chem. Commun.* **1983**, 675. – [1e] B. Delley, M. C. Manning, D. E. Ellis, J. Berkowitz, W. C. Trogler, *Inorg. Chem.* **1982**, *21*, 2247. – [1f] J. W. Lauher, *J. Am. Chem. Soc.* **1986**, *108*, 1521. – [1g] D. Braga, A. Roger, B. F. G. Johnson, *Inorg. Chim. Acta* **1990**, *174*, 185. – [1h] A. Sironi, *Inorg. Chem.* **1992**, *31*, 299. – [1i] P. T. Chesky, M. B. Hall, *Inorg. Chem.* **1983**, *22*, 2998. – [1j] R. D. Barreto, T. P. Fehlner, L.-Y. Hsu, S. G. Shore, *Inorg. Chem.* **1986**, *25*, 3572.

– [1k] M. A. Gallop, M. P. Gomez-Sal, C. E. Housecroft, B. F. G. Johnson, J. Lewis, S. M. Owen, P. R. Raithby, A. H. Wright, *J. Am. Chem. Soc.* **1992**, *114*, 2502. – [1l] J.-F. Halet, J.-Y. Saillard, R. Lissillour, M. J. McGlinchey, G. Jaouen, *Inorg. Chem.* **1985**, *24*, 218. – [1m] G. L. Griewe, M. B. Hall, *Inorg. Chem.* **1988**, *27*, 2250. – [1n] F. A. Cotton, X. Feng, *Inorg. Chem.* **1991**, *30*, 3666. – [1o] R. L. DeKock, K. S. Wong, T. P. Fehlner, *Inorg. Chem.* **1982**, *21*, 3203. – [1p] C. Mealli, *J. Am. Chem. Soc*. **1985**, *107*, 2245. – [1q] A. R. Pinhas, T. A. Albright, P. Hofmann, R. Hoffmann, *Helv. Chim. Acta* **1980**, *63*, 29.

[2] E. Hunstock, C. Mealli, M. J. Calhorda, J. Reinhold, *Inorg. Chem.* **1999**, *38*, 5053.

[3] [3a] *The Chemistry of Metal Cluster Complexes* (Eds.: D. F. Shriver, H. D. Kaesz, R. D. Adams), VCH, Cambridge, **1990**. – [3b] *Catalysis by Di- and Polynuclear Metal Cluster Complexes* (Eds.: R. D. Adams, F. A. Cotton), Wiley-VCH, Canada, **1998**.

[4] [4a] D. Braga, F. Grepioni, M. J. Calhorda, L. F. Veiros, *Organometallics* **1995**, *14*, 1992. – [4b] D. Braga, F. Grepioni, M. J. Calhorda, H. Wadepohl, S. Gebert, L. F. Veiros, *Organometallics* **1995**, *14*, 5350.

[5] J.-F. Riehl, N. Koga, K. Morokuma, *Organometallics* **1993**, *12*, 4788.

[6] [6a] J. Nijhoff, F. Hartl, J. W. M. van Outersterp, D. J. Stufkens, M. J. Calhorda, L. F. Veiros, *J. Organomet. Chem.***1999**, *573*, 121. – [6b] F. Hartl, J. W. M. van Outersterp, D. J. Stufkens, manuscript in preparation.

[7] R. G. Parr, W. Young, *Density Functional Theory of Atoms and Molecules,* Oxford University Press, New York, **1989**.

[8] [8a] R. Hoffmann, *J. Chem. Phys.* **1963**, *39*, 1397. – [8b] R. Hoffmann, W. N. Lipscomb, *J. Chem. Phys.* **1962**, *36*, 2179.

[9] [9a] J. Nijhoff, M. J. Bakker, F. Hartl, D. J. Stufkens, W.-F. Fu, R. van Eldik, *Inorg. Chem.* **1998**, *37*, 661. – [9b] J. W. M. van Outersterp, Garriga, M. T. Oostenbrink, H. A. Nieuwenhuis, D. J. Stufkens, F. Hartl, *Inorg. Chem.* **1995**, *34*, 6312. – [9c] J. Nijhoff, M. J. Bakker, F. Hartl, D. J. Stufkens, *J. Organomet. Chem.* **1999**, *572*, 271. – [9d] J. Nijhoff, F. Hartl, D. J. Stufkens, *Organometallics* **1999**, *18*, 4380.

[10] [10a] D. J. Stufkens, M. P. Aarnts, J. Nijhoff, B. D. Rossenaar, A. Vlček Jr., *Coord. Chem. Rev.* **1998**, *171*, 93. – [10b] D. J. Stufkens, A. Vlček Jr., *Coord. Chem. Rev.* **1998**, *177*, 127.

[11] R. Zoet, T. B. H. Jastrzebski, G. van Koten, T. Mahabiersing, K. Vrieze, D. Heijdenrijk, C. H. Stam, *Organometallics* **1988**, *7*, 2108.

[12] M. J. Frisch, G. W. Trucks, H. B. Schlegel, P. M. W. Gill, B. G. Johnson, M. A. Robb, J. R. Cheeseman, T. A. Keith, G. A. Petersson, J. A. Montgomery, K. Raghavachari, M. A. Al-Daham, V. G. Zakrzewski, J. V. Ortiz, J. B. Foresman, J. Cioslowski, B. B. Stefanov, A. Nanayakkara, M. Challacombe, C. Y. Peng, P. A. Ayala, W. Chen, M. W. Wong, J. L. Andres, E. S. Replogle, R. Gomperts, R. L. Martin, D. J. Fox, J. S. Binkley, D. J. Defrees, J. Baker, J. P. Stewart, M. Head-Gordon, C. Gonzalez, J. A. Pople, *Gaussian 94*, Gaussian Inc., Pittsburgh, PA, **1994**.

[13] R. Zoet, G. van Koten, K. Vrieze, A. J. M. Duisenberg, A. L. Spek, *Inorg. Chim. Acta*, **1988**, *148*, 71.

[14] N. E. Leadbeter, J. Lewis, P. R. Raithby, G. N. Ward, *J. Chem. Soc., Dalton Trans.* **1997**, 2511.

[15] For $Os_3(CO)_{10}$(*i*Pr-DAB) the lowest-energy absorption band is found at λ_{max} = 522 nm in toluene, THF, acetone, acetonitrile and pyridine. Bakker, M. J., Undergraduate scientific report, University of Amsterdam, 1996.

[16] M. P. Aarnts, M. P. Wilms, K. Peelen, J. Fraanje, K. Goubitz, F. Hartl, D. J. Stufkens, E. J. Baerends, A. Vlček, *Inorg. Chem.* **1996**, *35*, 5468.

[17] *Amsterdam Density Functional (ADF) program*, release 2.01 Vrije Universiteit: Amsterdan, The Netherlands, **1995**.

[18] [18a] E. J. Baerends, D. Ellis, P. Ros, *Chem. Phys.* **1973**, *2*, 41. – [18b] E. J. Baerends, P. Ros, *Int. J. Quantum Chem.* **1978**, *S12*, 169. – [18c] P. M. Boerrigter, G. te Velde, E. J. Baerends, *Int. J. Quantum Chem.* **1988**, *33*, 87. – [18d] G. te Velde, E. J. Baerends, *J. Comp. Phys.* **1992**, *99*, 84.

[19] S. H. Vosko, L. Wilk, M. Nusair, *Can. J. Phys.* **1980**, *58*, 1200.

[20] [20a] A. D. Becke, *J. Chem. Phys.* **1987**, *88*, 1053. – [20b] A. D. Becke, *Phys. Rev.* **1988**, *A38*, 3098.

[21] [21a] J. P. Perdew, *Phys. Rev.* **1986**, *B33*, 8822. – [21b] J. P. Perdew, *Phys. Rev.* **1986**, *B34*, 7406.

[22] [22a] L. Versluis, T. Ziegler, *J. Chem. Phys.* **1988**, *88*, 322. – [22b] L. Fan, T. Ziegler, *J. Chem. Phys.* **1991**, *95*, 7401.

[23] [23a] T. Ziegler, V. Tschinke, E. J. Baerends, J. G. Snijders, W. Ravenek, J. Phys. *Chem.* **1989**, *93*, 3050. – [23b] J. G. Snijders, E. J. Baerends, *Mol. Phys.* **1978**, *36*, 1789. – [23c] J. G. Snijders, E. J. Baerends, P. Ros, *Mol. Phys.* **1979**, *38*, 1909.

[24] P. J. Hay, W. R. Wadt, *Technical Report*, Los Alamos National Laboratory, **1990.**

[25] P. J. Hay, W. R. Wadt, *J. Chem. Phys.* **1985**, *82*, 299.

[26] J. H. Ammeter, H.-J. Bürgi, J. C. Thibeault, R. Hoffmann, *J. Am. Chem. Soc.* **1978**, *100*, 3686.

Received April 17, 2000
[I00155]